Fuel 218 (2018) 247–257

Contents lists available at ScienceDirect

Fuel

journal homepage: www.elsevier.com/locate/fuel

Full Length Article

High-pressure pyrolysis and oxidation of ethanol

Hamid Hashemi*, Jakob M. Christensen, Peter Glarborg

[a] DTU Chemical Engineering, Technical University of Denmark, DK-2800 Lyngby, Denmark

ARTICLE INFO

Keywords:
Ethanol
Ignition
High pressure
Reaction mechanism

ABSTRACT

The pyrolysis and oxidation of ethanol has been investigated at temperatures of 600–900 K, a pressure of 50 bar and residence times of 4.3–6.8 s in a laminar flow reactor. The experiments, conducted with mixtures highly diluted in nitrogen, covered fuel-air equivalence ratios (Φ) of 0.1, 1.0, 43, and ∞. Ethanol pyrolysis was observed at temperatures above 850 K. The onset temperature of ethanol oxidation occurred at 700–725 K over a wide range of stoichiometries. A considerable yield of aldehydes was detected at intermediate temperatures. A detailed chemical kinetic model was developed and evaluated against the present data as well as ignition delay times and flame speed measurements from literature. The model predicted the onset of fuel conversion and the composition of products from the flow reactor experiments fairly well. It also predicted well ignition delays above 900 K whereas it overpredicted reported flame speeds slightly. The results of sensitivity analyses revealed the importance of the reaction between ethanol and the hydroperoxyl radical for ignition at high pressure and intermediate temperatures. An accurate determination of the rate coefficients for this reaction is important to improve the reliability of modeling predictions.

1. Introduction

In recent years, ethanol has attracted both scientific and commercial attention as an additive to conventional liquid fuels or even as a alternative neat fuel. Gasoline doped with ethanol is widely used in spark-ignited (SI) engines [1]. Ethanol addition to gasoline promotes the overall octane number of the fuel while it potentially reduces the emission of particulate matter [2,3] and CO [4]. Ethanol addition to diesel fuels has also been studied [5,6] and a positive effect on fuel economy was found [5].

The relatively high energy density of ethanol makes it attractive also as a neat fuel. Using ethanol-based fuels produced from bio-sources can reduce the pressure on fossil fuels resources and reduce CO_2 release to the atmosphere. However, a widespread usage of ethanol as a fuel may increase the emission of aldehydes [1,4,7], which can cause health risks.

Compared to studies of hydrocarbon oxidation, research in the oxidation chemistry of oxygenated fuels is more recent, motivated by their importance in engines. In addition to the interest due to its role as a fuel or fuel additive, the reaction mechanism of ethanol is a crucial part in models for heavier alcohols often found in complicated biofuels [1]. Due to its relevance, e.g., for homogeneous-charge compression-ignition (HCCI) engines [8], ethanol ignition has been studied at high pressure and intermediate temperatures in flow reactors, rapid compression machines (RCM), and, to some extent, in shock tubes.

Data from high-pressure turbulent flow reactors are available for ethanol pyrolysis (950 K, 3–12 atm) [9] and ethanol oxidation (523–903 K, 12.5 atm) [10]. Ignition delay times at intermediate temperatures are mostly obtained in rapid compression machines (RCM),but the relatively short ignition delays of ethanol make it possible to conduct such experiments also in shock tubes. Ignition delay data from RCM have been reported by Lee et al. [11] (750–1000 K, 20–40 atm), Mittal et al. [12] (825–985 K, 10–50 bar), Lee et al. [13] (700–1300 K, 67–80 bar), and Barraza-Botet et al. [14] (880–1150 K, 3–10 atm), while shock tube ignition delays are available from Noorani et al. [15] (1070–1760 K, 2–12 atm), Heufer and Olivier [16] (800–1400 K, ⩽40 bar), and Cancino et al. [17] (650–1220 K, 10–50 bar). Some of these studies cover partly the pressure and temperatures of the current study, but ignition delay times provide only an overall characteristic of combustion. Additional insight into the combustion chemistry can be obtained by measuring more detailed characteristics such as species profiles.

A number of chemical kinetic models for ethanol oxidation has been published over the years [10,12,13,18–25], but only some of them have been applied at elevated pressure. Marinov [21] conducted the first comprehensive modeling study of ethanol oxidation, estimating a number of rate constants by analogy to known reactions. Whereas most of the data used for validation were obtained at low pressures and high

* Corresponding author.
E-mail address: hah@kt.dtu.dk (H. Hashemi).
URL: http://www.kt.dtu.dk (H. Hashemi).

https://doi.org/10.1016/j.fuel.2017.12.085
Received 3 October 2017; Received in revised form 15 December 2017; Accepted 19 December 2017

temperatures, his model has been adopted also for high-pressure studies [15]. Dryer and co-workers [10,22] developed a kinetic model and validated it against flow-reactor data at 12.5 bar as well as against ignition delays up to 50 bar. This model was largely adopted by Lee et al. [13] who extended the validation range to 77 bar. Cancino et al. [17] modified earlier kinetic models to address ethanol oxidation chemistry at high pressures and intermediate temperatures. However, their model was solely validated against shock tube data. Mittal et al. [12] optimized a model for ethanol oxidation at intermediate temperatures.

By the advent of more reliable data for the key reactions in ethanol oxidation, a careful reevaluation of reactions focusing on medium temperatures and high pressure seems desirable. In this paper we present species concentration profiles from ethanol pyrolysis and oxidation in a flow reactor at high pressure and intermediate temperatures. A detailed chemical kinetic model based on earlier high-pressure studies from our laboratory [26–33] is extended with a subset for ethanol oxidation and evaluated against the data from the present work as well as from literature.

2. Experimental approach

The experiments were conducted in a laboratory-scale high-pressure laminar-flow reactor designed to approximate plug flow [26]. The setup was described in detail elsewhere [26] and only a brief description is provided here. The system was used here for the investigation of ethanol oxidation chemistry at a pressure of 50 bar, temperatures up to 900 K, and a flow rate of 4.78 Nliter/min (4.42 Nliter/min for the pyrolysis experiments, STP: 1 atm and 273.15 K).

The reactions took place in a tubular quartz reactor (inner diameter of 8 mm), enclosed in a stainless steel tube that acted as a pressure shell. The system was pressurized from the feed gas cylinders and the reactor pressure was monitored upstream of the reactor by a differential pressure transducer and controlled by a pneumatically operated pressure control valve positioned after the reactor. The pressure fluctuations of the reactor were limited to ± 0.2%. The pressure in the shell-side of the reactor was retained close to that inside the reactor in order to prevent breaking the quartz tube.

The steel tube was placed in a tube oven with three individually controlled electrical heating elements that produced an isothermal reaction zone (± 6 K) of 42–48 cm in the middle of the reactor. A moving thermocouple was used to measure the temperature profile inside the pressure shell at the external surface of the quartz tube after stabilizing the system.

The liquid feeding system is described in detail elsewhere [34]. The liquid was pressurized by an HPLC pump and its flow to the reactor was controlled by a liquid mass flow controller. The liquid was mixed with the incoming gas and heated to temperatures around 520 K in evaporator before entering the reactor. A tube of more than 4 m in the evaporator ensured sufficient time for evaporation and mixing. A long stabilization period prior to each test served to limit the fluctuations of the liquid feeding system to ± 5%.

Downstream of the reactor, the system pressure was reduced to atmospheric level prior to product analysis, which was conducted by an on-line *6890N Agilent Gas Chromatograph* (GC-TCD/FID) calibrated according to the procedure in [32]. The GC allowed detection of O_2, CO, CO_2, C_2H_4 and C_2H_6 with estimated uncertainties around 10%. The uncertainty for ethanol was higher due to its calibration procedure. Methane could not be quantified accurately due to signal overlapping with CO. Distinguishing methanol from acetaldehyde was not possible due to signal overlapping for the GC configuration used. However, it was possible to measure the signal areas corresponding to sum of these components. Using the response factor of acetaldehyde, the sum of acetaldehyde and methanol was estimated but a relatively large uncertainty must be acknowledged. Moreover, due to the small signal to noise ratio of formaldehyde, a larger uncertainty especially in measuring low quantities of formaldehyde was expected.

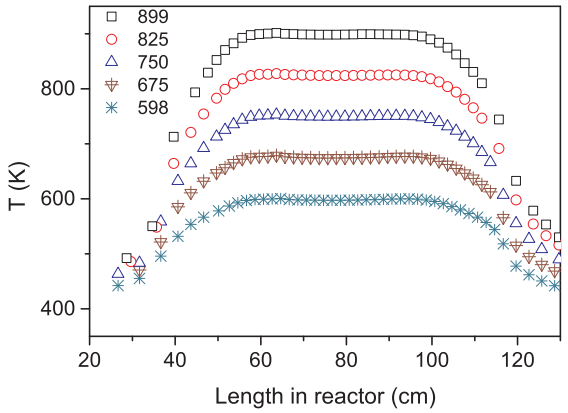

Fig. 1. Measured temperature profiles across the reaction zone. The nitrogen flow rate was 4.78 NL/min at a pressure of 50 bar. The flow rate and temperature profiles were slightly different for the ethanol pyrolysis experiments.

All gases used in the present experiments were high purity gases or mixtures with certified concentrations (± 2% uncertainty) and the ethanol purity was above 99.8%. The total flow rate was measured by a bubble flow meter downstream of the reactor.

For each set of experiments, the concentrations of reactants as well as the pressure of the system were maintained while the temperature of the isothermal zone was increased in small steps. Fig. 1 shows the measured temperature profiles for different isotherms in pure nitrogen. The residence time of the gases in the isothermal zone of the reactor can be estimated as τ[s] = 3840/T [K] (± 8%) for all the oxidizing experiments and τ[s] = 4098/T [K] (± 8%) for the pyrolysis tests.

The temperature rise due to exothermic reactions was limited by strongly diluting the reactants in nitrogen. The adiabatic temperature increase was estimated to a maximum of 107 K. However, measurements of the temperature profile under oxidizing conditions indicated only a marginal difference compared to the flow of pure nitrogen. This is attributed to a fast heat transfer between the quartz reactor and its surrounding, facilitated by the small diameter of the quartz tube.

The possible impact of surface reactions is a concern in flow reactor studies. In this work, surface reactions were minimized, partly by the use of quartz as reactor material and partly by the high pressure, inhibiting diffusion to the wall. Previous work in the reactor, covering a range of fuels [26,29–33,35,36], have shown no indications of wall reactions. In a recent study of oxidation of ammonia [36], known to be sensitive to surfaces, we found that replacing the quartz reactor by an alumina reactor did not affect the oxidation behavior. Hence, it seems safe to assume a negligible contribution from surface reactivity on the gathered data.

3. Chemical kinetic model

The reaction mechanism and the corresponding thermodynamic and transport data were based on previous work by the authors on high-pressure oxidation of hydrogen [31], methane [32], acetylene [35], ethylene [29], ethane [33], and methanol [30]. The acetaldehyde subset is reviewed in a companion paper [37]. Here, the reactions important for ethanol oxidation at high pressure and moderate temperatures are discussed. Selected reactions are listed in Table 1.

The thermal decomposition of ethanol (R1), a key reaction at high temperatures [10], is believed to proceed through three channels [38]:

$$CH_3CH_2OH(+M) = C_2H_4 + H_2O(+M) \quad \text{(R1a)}$$

$$= CH_3 + CH_2OH(+M) \quad \text{(R1b)}$$

$$= C_2H_5 + OH(+M) \quad \text{(R1c)}$$

We have adopted the rate coefficients from Sivaramakrishnan et al. [38], who combined measurements of ethanol dissociation over

Table 1
Reactions from ethanol reaction mechanism. The rate constants are in the form of $k = A\,T^n \exp(-E/(RT))$. Units are mol, cm, K, s, and cal.

	Reaction	A	n	E	Note/Ref.
R1a	$CH_3CH_2OH = C_2H_4 + H_2O$	3.8E20	−2.060	69,426	[38][a]
R1b	$CH_3CH_2OH = CH_3 + CH_2OH$	1.8E47	−8.960	101,002	[38][a]
R1c	$CH_3CH_2OH = C_2H_5 + OH$	6.2E51	−10.340	109,879	[38][a]
R2a	$CH_3CH_2OH + H = CH_3CHOH + H_2$	8.8E03	2.680	2913	[38]
R2b	$CH_3CH_2OH + H = CH_2CH_2OH + H_2$	5.3E03	2.810	7491	[38]
R2c	$CH_3CH_2OH + H = CH_3CH_2O + H_2$	9.5E02	3.140	8696	[38]
R3a	$CH_3CH_2OH + OH = CH_3CHOH + H_2O$	6.9E16	−0.733	13,799	[39], see text
	duplicate rate constant	4.6E05	2.147	−1779	
R3b	$CH_3CH_2OH + OH = CH_2CH_2OH + H_2O$	2.4E10	0.881	5350	[39], see text
	duplicate rate constant	9.6E05	1.927	−831	
R3c	$CH_3CH_2OH + OH = CH_3CH_2O + H_2O$	7.9E06	1.609	−461	[39], see text
	duplicate rate constant	1.6E03	2.870	53	
R4a	$CH_3CH_2OH + HO_2 = CH_3CHOH + H_2O_2$	8.2E03	2.550	10,750	[21]
R4b	$CH_3CH_2OH + HO_2 = CH_2CH_2OH + H_2O_2$	1.2E04	2.550	15,750	[21]
R4c	$CH_3CH_2OH + HO_2 = CH_3CH_2O + H_2O_2$	2.5E12	0.000	24,000	[21]
R5a	$CH_3CH_2OH + CH_3 = CH_3CHOH + CH_4$	2.0E01	3.370	7630	[40]
R5b	$CH_3CH_2OH + CH_3 = CH_2CH_2OH + CH_4$	2.0E00	3.570	7717	[40]
R5c	$CH_3CH_2OH + CH_3 = CH_3CH_2O + CH_4$	3.3E02	3.300	12,283	[40]
R6a	$CH_3CHOH(+M) = CH_3CHO + H(+M)$	6.2E09	1.310	33,778	[41]
	Low-pressure limit:	1.8E16	0.000	20,782	
	Troe parameters: 0.187 65.2 2568 41,226				
R6b	$CH_3CHOH(+M) = CH_2CHOH + H(+M)$	6.4E09	1.330	35,974	[41]
	Low-pressure limit:	8.2E14	0.000	21,517	
	Troe parameters:0.473 10 2218 2615				
R6c	$CH_3CHOH(+M) = CH_3 + CH_2O(+M)$	2.2E09	1.180	33,987	[41]
	Low-pressure limit:	5.9E15	0.000	21,333	
	Troe parameters: 0.124 1 1729 50,000				
R7a	$CH_3CHOH + H = CH_2CHOH + H_2$	3.1E12	0.270	−334	[42]
R7b	$CH_3CHOH + H = C_2H_4 + H_2O$	1.6E20	−1.810	9448	[42][a]
R7c	$CH_3CHOH + H = CH_3 + CH_2OH$	4.0E23	−2.527	13,637	[42][a]
R7d	$CH_3CHOH + H = C_2H_5 + OH$	6.3E21	−2.110	15,269	[42][a]
R7e	$CH_3CHOH + H = CH_3CH_2OH$	1.6E40	−7.820	12,916	[42,43][a]
R8a	$CH_3CHOH + O_2 = CH_3CHO + HO_2$	3.8E20	−2.429	3090	[44][a]
R8b	$CH_3CHOH + O_2 = CH_2CHOH + HO_2$	4.4E05	1.699	2330	[44][a]
R9a-rev	$C_2H_4 + OH = CH_2CH_2OH$	6.0E37	−7.440	14,269	[45][a]
	duplicate rate constant	2.8E19	−2.410	1011	[a]
R9b	$CH_2CH_2OH = CH_2CHOH + H$	2.7E27	−4.440	37,205	[46][a]
R10a	$CH_2CH_2OH + H = C_2H_4 + H_2O$	3.6E16	−0.716	8767	[42][a]
R10b	$CH_2CH_2OH + H = CH_2OH + CH_3$	7.5E20	−1.690	13,429	[42][a]
R10c	$CH_2CH_2OH + H = C_2H_5 + OH$	8.1E19	−1.510	15,534	[42][a,b]
R11a	$CH_2CH_2OH + O_2 = CH_2CHOH + HO_2$	1.9E30	−5.510	16616.0	[47][a]
	duplicate rate constant	6.0E03	−10.000	199.0	[47][a]
R11b	$CH_2CH_2OH + O_2 = HOCH_2CH_2OO$	4.2E26	−4.460	3940	[47][a]
R11c	$CH_2CH_2OH + O_2 = CH_2O + CH_2O + OH$	1.2E29	−5.440	11,323	[47][a]
R12	$HOCH_2CH_2OO = CH_2O + CH_2O + OH$	3.8E18	−2.600	19,972	[47][a]
R13	$CH_3CH_2O(+M) = CH_3 + CH_2O(+M)$	6.3E10	0.930	17,098	[41]
	Low-pressure limit:	4.7E25	0.930	16,532	
	Troe parameters: 0.426 0.3 2278 100,000				
R14a	$CH_3CH_2O + H(+M) = CH_3CH_2OH(+M)$	3.1E11	0.894	13	[48]
	Low-pressure limit:	3.8E51	−15.550	11,101	
R14b	$CH_3CH_2O + H(+M) = CH_2OH + CH_3(+M)$	2.6E18	−1.050	5128	[48]
	Low-pressure limit:	3.0E11	0.893	17	
R14c	$CH_3CH_2O + H = CH_3CHO + H_2$	7.5E09	1.150	673	[48]

[a] At 100 atm pressure, for other pressures see the mechanism file in the supplementary materials.
[b] For reactions between CH_2CH_2OH and other radicals (estimated by analogy to C_2H_5 reactions), see the mechanism file in the supplementary materials.

1392–1663 K with a theoretical treatment. The results of Wu et al. [49], obtained at 1450–1760 K in shock-tube tests with very low ethanol concentrations of 1–3 ppm, indicate that the branching ratios for R1 may be less sensitive to pressure than predicted by Sivaramakrishnan et al. [38], but more work is needed to confirm this. More recently, Kiecherer et al. [50] extracted the rate of the $C_2H_4 + H_2O$ channel (R1a) at 1300–1510 K and atmospheric pressure; their measurements support those of Sivaramakrishnan et al. [38] and Wu et al. [49].

Ethanol oxidation is controlled by H-abstraction reactions forming isomers of C_2H_5O radicals, i.e., α-hydroxyethyl (CH_3CHOH), β-hydroxyethyl (CH_2CH_2OH), and ethoxy (CH_3CH_2O). The abstraction by H from ethanol (R2),

$$CH_3CH_2OH + H = CH_3CHOH + H_2 \quad \text{(R2a)}$$

$$= CH_2CH_2OH + H_2 \quad \text{(R2b)}$$

$$= CH_3CH_2O + H_2 \quad \text{(R2c)}$$

is challenging to measure, as the H-decay may be affected by thermal dissociation of ethanol at high temperatures. To overcome this problem, Sivaramakrishnan et al. [38] measured the D atom concentration in the reaction $CH_3CH_2OH + D$ over 1054–1359 K and then eliminated the isotope effect via theoretical calculations. Their results, adopted in this work, show that the dominant channels form CH_3CHOH (R2a) and CH_2CH_2OH (R2b).

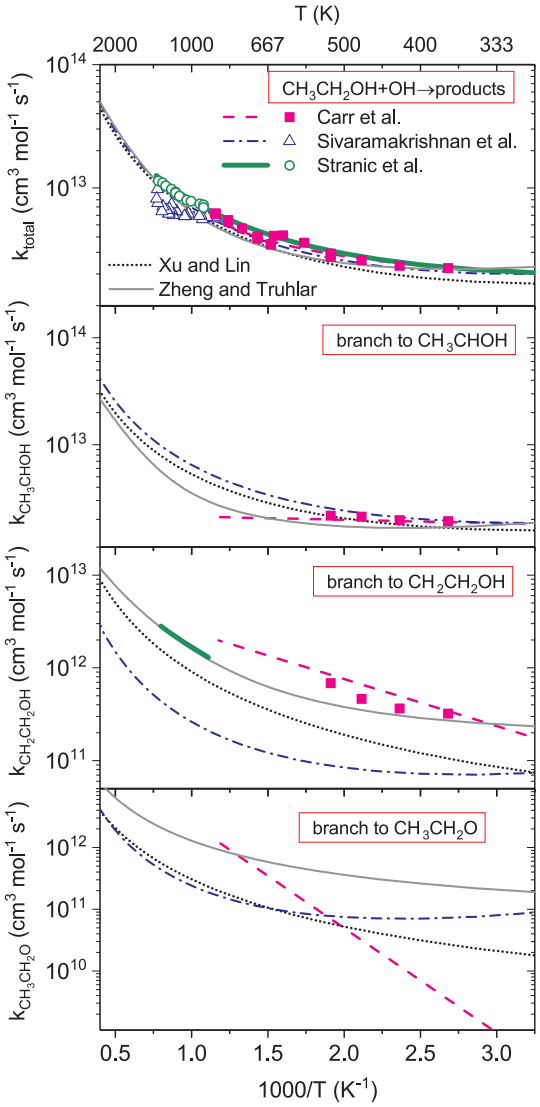

Fig. 2. The rate constant for R3 (CH_3CH_2OH + OH → products). Literature data are taken from Sivaramakrishnan et al. [51], Carr et al. [52], Xu and Lin [38], Stranic et al. [53], and Zheng and Truhlar [39]. Symbols mark measured data and lines denote the results of theoretical calculation or evaluation.

The reaction between ethanol and the hydroxyl radical (R3), which is the dominant H-abstraction reaction of ethanol at intermediate temperatures [10,51], has been investigated by several research groups recently [38,39,51–53]. Fig. 2 shows an Arrhenius plot for the overall reaction, as well as for each of the three product channels. Determinations of the overall rate constant [38,51,53], covering a wide range of temperature, are in fairly good agreement, but reported values for the product branching fraction vary significantly.

The CH_2CH_2OH radical produced from R3b is expected to dissociate to C_2H_4 + OH at temperatures above 550 K [38]. Above 650 K, the dissociation further accelerates, so it is considered instantaneous compared to other chemical time scales. Sivaramakrishnan et al. [38] measured the OH-decay rate, which represents an overall rate for R3a + R3c, over 857–1297 K. Their calculated rate for R3a + R3c was larger than the measured values, so they adjusted the barrier heights of all the branches in their calculations to compensate for it. Their proposed rate constants indicate negligible contributions from R3b and R3c in the overall rate of CH_3CH_2OH + OH at combustion temperatures.

Carr et al. [51] investigated reaction R3 at lower temperatures (298–865 K) using isotopic labelling to distinguish between different channels. Below 523 K, CH_2CH_2OH decomposition is small and channel R3b could be quantified, albeit with an increased uncertainty at elevated temperatures. Their results indicate that R3c is the dominant path, with minor contributions of the α and β channels.

More recently, Stranic et al. [53] measured the overall rate as well as the rate of the β branch of the title reaction over 900–1270 K. Isotopic labeling of OH radicals enabled Stranic et al. to account for interference from CH_2CH_2OH dissociation on the measured rate. The branching ratio of the β channel was reported to be 0.2–0.25 over 900–1200 K whereas distinction between R3a and R3c was not possible.

The theoretical study by Zheng and Truhlar [39] explains most of the reported observations over a wide range of temperature (Fig. 2) and we have adopted their recommended rate constants. Their calculated β branching ratio is close to the only reliable measurement at higher temperature from Stranic et al. [53] and also in good agreement with the data from Carr et al. [51]. To implement the calculated rate in CHEMKIN [54], a modified Arrhenius equation was fitted to the data over 300–3000 K with a maximum reproduction error of 3%.

For the reactions of HO_2 (R4) and CH_3 (R5) with ethanol, no experimental data have been reported. For CH_3CH_2OH + HO_2 (R4), which would be expected to be important for ignition at intermediate temperatures, we have adopted the rate constants from Marinov [21], estimated by analogy to similar reactions of methanol and propane.

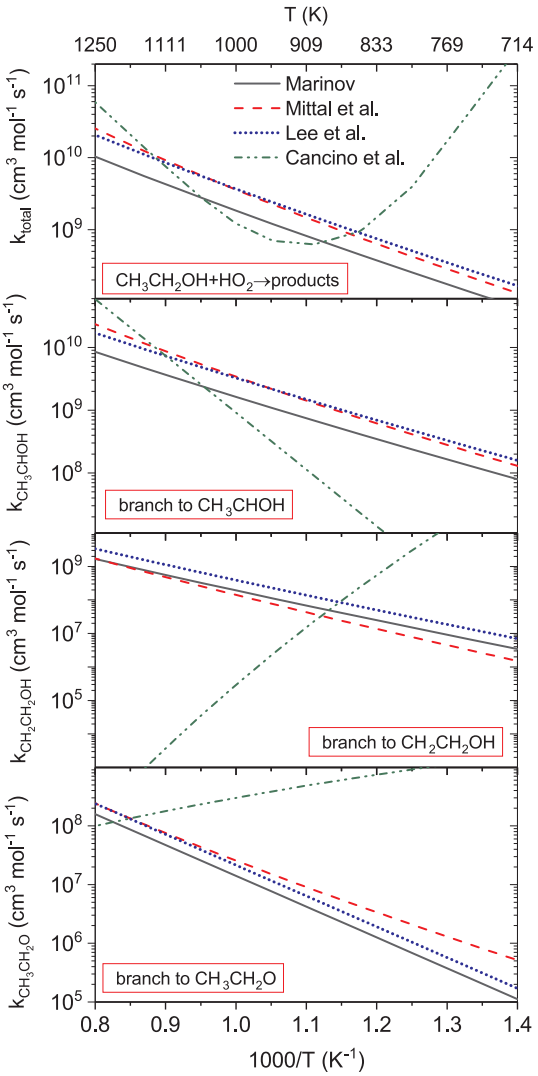

Fig. 3. The rate constant for R4 (CH_3CH_2OH + HO_2 → products). Literature data are taken from Lee et al. [21], Cancino et al. [17], Marinov [13], and Mittal et al. [12]. Symbols mark measured data and lines denote the results of theoretical calculation or evaluation.

Recent studies of ignition delay times of ethanol [12,13,17] generally employ values of the overall rate constant and branching ratio for reaction R4 in fair agreement with the estimates from Marinov [21]; only the data from Cancino et al. [17] show significant differences (see Fig. 3) and should probably be used with caution. However, a more reliable determination of the rate coefficients for this reaction is desirable. For the reaction between ethanol and methyl (R5), we rely on data from the theoretical study by Xu et al. [40].

The α-hydroxyethyl radical (CH_3CHOH) is presumably the major product of H-abstraction from ethanol. For the decomposition of CH_3CHOH (R6), the rate constants are taken from an RRKM study by Dames [41] who predicted the major branch, CH_3CHOH (+M) = CH_3CHO + H (+M) (R6a) to be faster by up to one order of magnitude compared to an earlier calculation by Xu et al. [46].

The reaction between CH_3CHOH and atomic hydrogen (R7) is expected to be important only at low pressures [42]. The rate constants for the different branches of this reaction (see Table 1) are taken from a theoretical study by Labbe et al. [42].

For the reaction between CH_3CHOH and molecular oxygen, we rely on a theoretical study by da Silva et al. [44] who found the major products to be CH_3CHO + HO_2 under combustion conditions. The other possible products, CH_2CHOH + HO_2, were formed in small amounts and only at high temperatures. The high pressure limit of this reaction was also studied by Zador et al. [47] who predicted an overall rate larger within a factor of two. However, the pressure dependence of the reaction was not explored in [47].

The dissociation of the β-hydroxyethyl radical (CH_2CH_2OH) is expected to yield C_2H_4 + OH (R9a) or CH_2CHOH + H (R9b) [46]. The branch to C_2H_4 was studied theoretically [45,46,55] and experimentally [56]. The theoretical derivations by Xu et al. [46] and Senosiain et al. [45] differed within a factor of six at atmospheric pressure over 700–1000 K. The larger sensitivity to temperature predicted by Senosiain et al. [45] was confirmed experimentally by Srinivasan et al. [56]. Therefore, the C_2H_4 + OH (R9a) branch is taken from Senosiain et al. [45] who fitted pressure-dependent rate constants for the reverse direction of this reaction. The rate constant of the minor branch to CH_2CHOH + H (R9b) is adopted from the calculations of Xu et al. [46].

Gimenez-Lopez et al. [29] proposed that the major consumption path of CH_2CH_2OH under conditions similar to the present study was its reaction with molecular oxygen. They estimated the rate constant of this reaction by analogy to C_2H_5 reactions. Here, we adopt the results of a more recent theoretical study by Zador et al. [47] who investigated the title reaction by using high-level ab initio calculations. Zador et al. calculated an overall high-pressure rate around five times larger than that estimated by Gimenez-Lopez et al. [29].

$$CH_2CH_2OH + O_2(+M) = CH_2CHOH + HO_2(+M) \quad \text{(R11a)}$$

$$= HOCH_2CH_2OO(+M) \quad \text{(R11b)}$$

$$= CH_2\ O + CH_2\ O + OH(+M) \quad \text{(R11c)}$$

The ethoxy radical (CH_3CH_2O) is mainly consumed by thermal dissociation to CH_3 + CH_2O (R13) under combustion conditions. Caralp et al. [57] measured the ethoxy radical decomposition at 391–471 K. We have adopted the rate coefficients from the RRKM study by Dames [41], covering temperatures of 400–1200 K and pressures of 0.001–100 atm. It should be noted that the earlier theoretical study of Xu et al. [46] resulted in substantially different pressure and temperature dependencies, and measurements at medium temperatures are desirable.

4. Results and discussion

4.1. Ethanol oxidation in the flow reactor

The aim of this work was to characterize the pyrolysis and oxidation of ethanol at high pressure and intermediate temperatures. Here, results from the flow reactor experiments are presented and compared to predictions by the developed model. For the calculations using Chemkin [54], a model with constrained temperature and pressure was used.

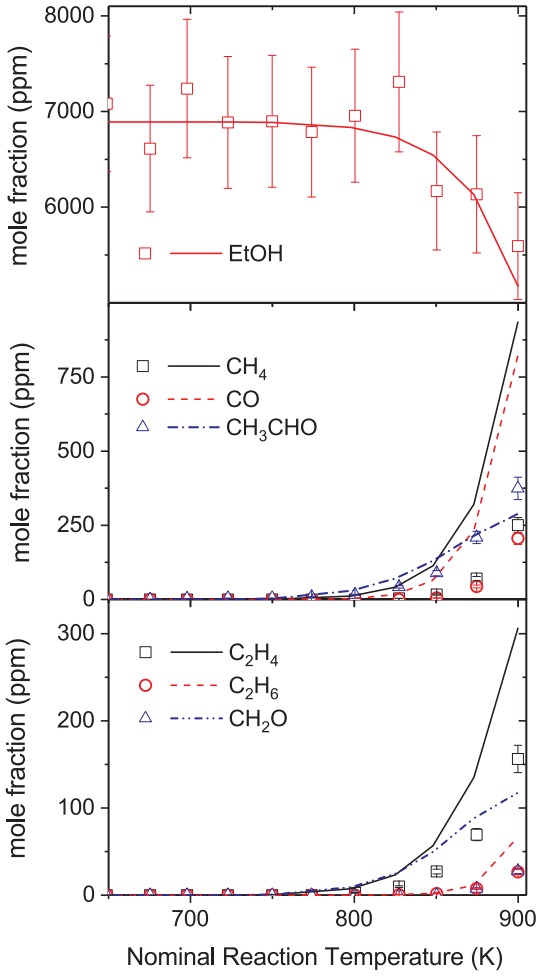

Fig. 4. Results of pyrolysis experiments (0.689% ethanol in N_2) at 50 bar. Gas residence time is given by τ[s] = 4098/T[K] (± 8%).

Fig. 4 shows the results of the pyrolysis experiments. The ethanol conversion starts around 825 K and increases with temperature to 18% at 900 K. The major detected products are CH_4, CO, and C_2H_4. The ethanol mole fraction fluctuates below the onset temperature of reaction, but these fluctuations are within the ±5% uncertainty of the liquid feeding system discussed earlier. Carbon is balanced within ± 9%, with the difference attributed partly to fluctuations in the liquid feeding system and partly to uncertainties in measuring aldehydes and ethanol.

The model predicts the onset temperature of ethanol decomposition well, but it slightly overestimates the reactivity of ethanol at higher temperatures. The acetaldehyde yield from the model agrees well with the measurements at temperature below 875 K. As discussed earlier, the GC configuration does not allow quantification of acetaldehyde and methanol separately. We expect the measured quantity to represent acetaldehyde, as the methanol yield predicted by the model is negligible.

The ethanol conversion starts around 700 K for the fuel-rich mixture (Φ = 43, see Fig. 5). Acetaldehyde and CO are the major detected products of ethanol partial oxidation. The methane concentration is not quantified due to peaks overlapping in GC signals. Similar to the pyrolysis test, the sum of methanol and acetaldehyde measured by GC is interpreted as acetaldehyde. The maximum conversion of ethanol is 36% while oxygen is fully consumed at high temperatures.

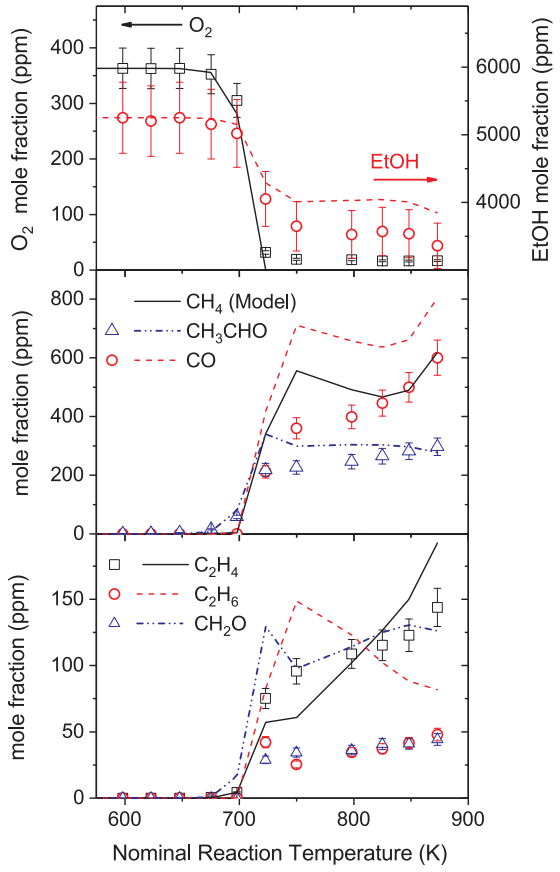

Fig. 5. Results of experiments under reducing conditions (0.525% ethanol and 0.0363% O_2 in N_2, $\Phi = 43$) at 50 bar. Gas residence time is given by τ[s] = 3840/T[K] (± 8%).

The model predicts well the onset temperature of reaction but it marginally underestimates the fuel conversion at high temperatures. Although the model overpredicts the concentrations of ethane and ethanol, it reproduces well the fractions of O_2, C_2H_4, and CH_3CHO. By adopting the methane concentration from the model, the carbon loss in the experiments is at most 18%.

Under stoichiometric conditions, ethanol oxidation starts around 725 K. The major detected products are CO and CO_2, as shown in Fig. 6. The CO concentration peaks around 750 K and decreases gradually at higher temperatures. Aldehydes are detected around 725 K, but disappear at higher temperatures. Ethene, detected in a few ppm, shows a non-monotonic behaviour toward temperature.

The model reproduces fairly well the onset of fuel conversion as well as the concentration of major products. Even though CO is overestimated at high temperatures, the non-linear changes in aldehydes and ethene profiles are well predicted by the model. Balancing carbon reveals a maximum loss of 26%.

For the fuel-lean mixture ($\Phi = 0.10$), the fuel oxidation is observed at temperatures above 725 K, similar to the onset temperature for stoichiometric and reducing mixtures. Again, aldehydes peak at 725 K, but they are soon depleted at higher temperatures. The model agrees well with to the measurements and the carbon is balanced within a maximum loss of 21% which occurs at 725 K (Fig. 7).

The data presented here are in line with the results by Haas et al. [10] who studied ethanol ignition at a lower pressure of 12.5 atm. They reported ignition temperatures of 750–775 K under stoichiometric ($\Phi = 0.91$, 0.27% ethanol) and fuel–lean ($\Phi = 0.43$, 0.28% ethanol) conditions. No sign of negative temperature coefficient (NTC) behavior was observed neither in their work nor in the present study.

The consumption paths of ethanol according to the model is shown in Fig. 8 for conditions representing the current experiments. Under all

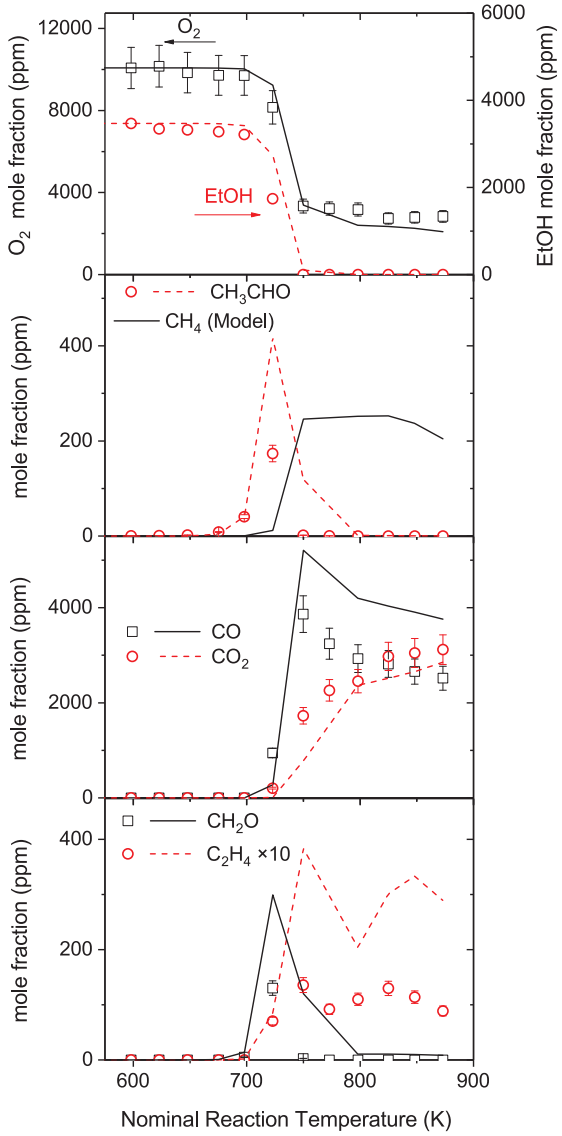

Fig. 6. Results of experiments under stoichiometric conditions (0.3467% ethanol and 1.01% O_2 in N_2, $\Phi = 1.0$) at 50 bar. Gas residence time is given by τ[s] = 3840/T[K] (± 8%).

investigated conditions, ethanol is mainly converted to the α-hydroxyethyl radical (CH_3CHOH). In the absence of oxygen, ethanol is mainly consumed by reaction with H (R2a) and CH3 (R5a). Under oxidizing conditiond, reactions with OH (R3a) and HO_2 (R4a) become dominant. The α-hydroxyethyl radical either reacts with an oxygen molecule (R8a) or dissociates (R6a), depending on the oxygen availability. Both paths yield acetaldehyde which is then dehydrogenated to form the acetyl radical (CH_3CO).

$$CH_3CHO + H = CH_3CO + H_2 \quad \text{(R16a)}$$

$$CH_3CHO + OH(+M) = CH_3CO + H_2O(+M) \quad \text{(R17b)}$$

$$CH_3CHO + HO_2 = CH_3CO + H_2O_2 \quad \text{(R18a)}$$

The acetyl radical then dissociates to form CO and CH_3 (R19).

Hydrogen abstraction from ethanol may also yield minor quantities of CH_3CH_2O or CH_2CH_2OH. The ethoxy radical dissociates to formaldehyde which finally gives CO.

$$CH_3CH_2O(+M) = CH_2\ O + CH_3(+M) \quad \text{(R13)}$$

$$CH_2\ O + OH = HCO + H_2O \quad \text{(R20)}$$

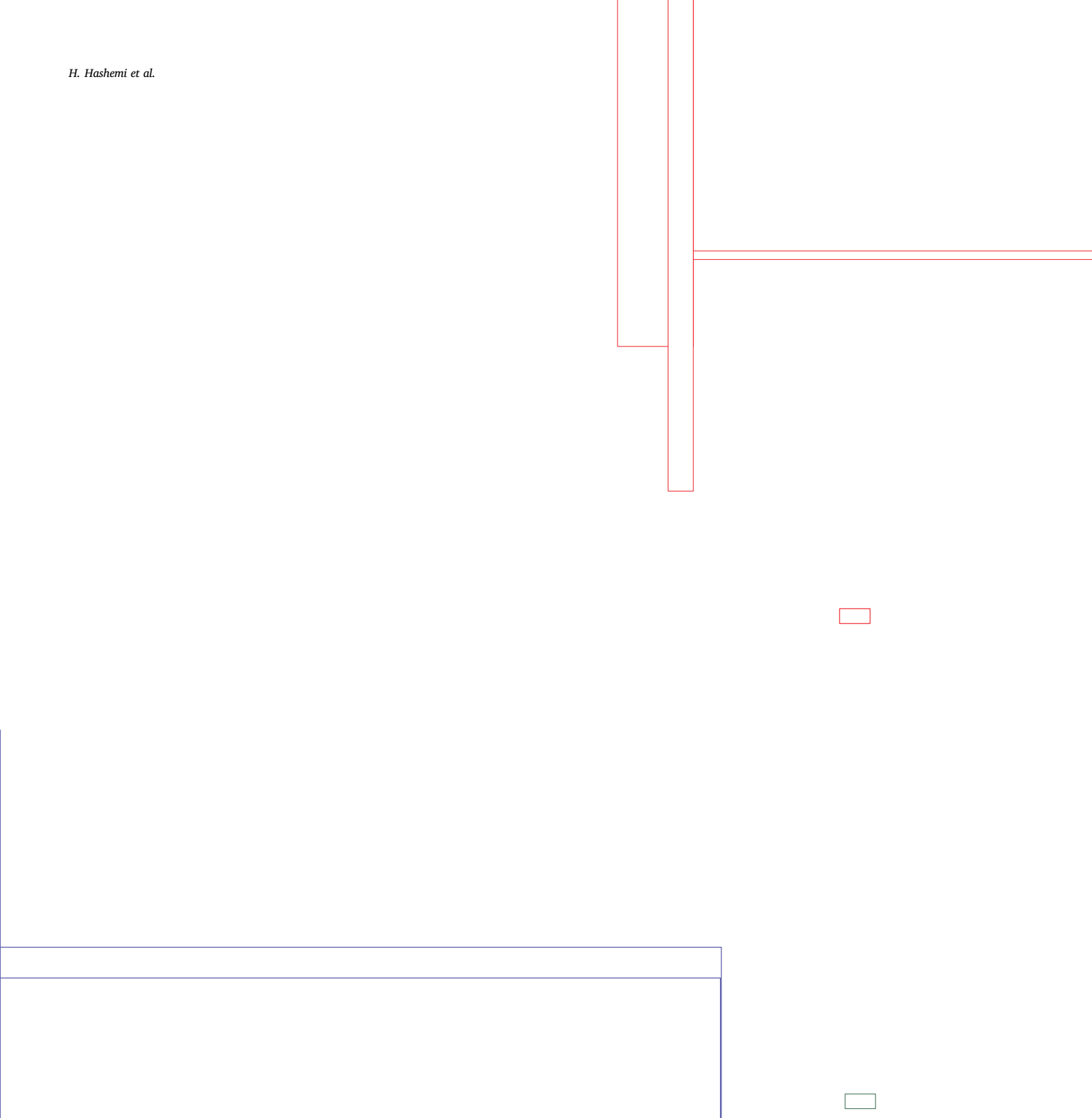

Fig. 9. Sensitivity of ethanol prediction by the model at 50 bar and under the flow reactor conditions for ethanol pyrolysis (PYR), fuel-rich (RD), stoichiometric (ST), and fuel-lean (OX) conditions. The coefficients are calculated at the time corresponding to 20% conversion of ethanol.

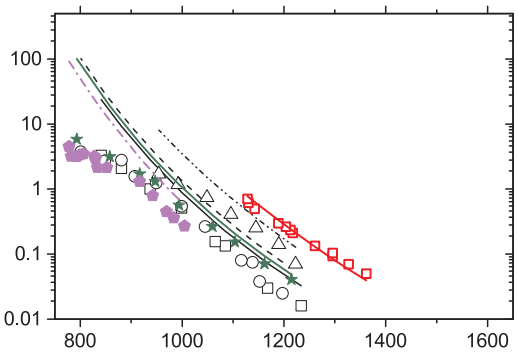

$$S_i = \frac{(\Delta X_{\mathrm{EtOH}}/X_{\mathrm{EtOH}})}{(\Delta k_i/k_i)} \quad (1)$$

Fig. 9 shows the results of the analysis under the flow reactor conditions. Ethanol pyrolysis is mainly sensitive to H-abstraction from ethanol by the hydrogen and methyl radicals (R2, R5), but also ethanol dissociation to CH_2OH (R1b) is important.

Under reducing conditions, in addition to R2 and R5, H-abstraction by OH (R3b) and HO_2 (R4a) becomes important. Dissociation of H_2O_2 promotes the oxidation at 723 K, but surprisingly it has an inhibiting effect at 873 K, even though it proceeds in the forward direction.

$$H_2O_2(+M) = OH + OH(+M) \quad (R23)$$

For both stoichiometric and oxidizing conditions, the H-abstraction by HO_2 (R4) governs the main fuel oxidation at 723 K. Abstraction by HO_2 and CH_3OO from acetaldehyde is also important for ethanol oxidation.

$$CH_3CHO + HO_2 = CH_3CO + H_2O_2 \quad (R24)$$

$$CH_3CHO + CH_3OO = CH_3CO + CH_3OOH \quad (R25)$$

4.2. Comparison with literature data

4.2.1. Ignition at higher temperatures

Fig. 10 compares ethanol ignition delays calculated here with those reported in literature [12–17]. The ignition delay decreases monotonically with increasing temperature and the model can predict the ignition delays fairly well for most of the cases above 900 K. However, it systematically overpredicts ignition delays measured in shock tube (top figure) at T < 900 K. However, the calculations agree better with measurements from RCM (bottom figure) at T < 900 K.

Fig. 11 compares the measurements from RCM and shock tubes at T < 1000 K. The slope of ignition delays from RCM is sharper compared to those observed in shock tubes, i.e., RCM ignition delays are more sensitive to temperature. The fraction of inert gas is different between experiments in shock tubes and RCM. Most of the shock-tube data were measured for ethanol/air mixtures, while in the RCM experiments more-diluted mixtures were tested. However, the difference in initial fraction cannot be the source of the observed considerable scatter among the data. According to the model (not shown here) we expect $\tau \sim 1/X_{EtOH}$, where τ and X_{EtOH} are ignition delay time and molar fraction of ethanol, respectively.

The difference between RCM and shock tube data might be due to the pre-ignition pressure rise in shock tube experiments, as noted earlier [12,13]. Over long residence times, pressure and temperature increase gradually behind the shock wave [13], even in non-reactive mixtures [58,59]. These pre-ignition effects are believed to be fuel-dependent and increase at lower temperatures [13]. Lee et al. [13] found that the ignition of ethanol in shock tubes is non–homogeneous due to local hot-spots and is highly affected by pre-ignition effects. In RCM, on the other hand, it is common to observe decreasing pressure (and temperature) due to heat transfer. In general, it is required to include those pre-ignition pressure variation in interpreting and simulating data for long residence time for both shock tubes and RCM. In the RCM data simulated here, the pre-ignition pressure-drop was reported to be fairly small and therefore is not included in the simulation. For the shock tube data from Cancino et al. [17], simulations are repeated by considering a pressure rise of 2% (per ms) behind the shock wave. The results (not shown here) improve but still deviate considerably from the measurements at T < 900 K. We attribute the differences at least partly to device-dependent non-idealities in conducting experiments. More-controlled experiments in RCM and shock tubes might help to find the source of the data discrepancy at low temperature and high pressure.

The sensitivity of the predicted ignition delay to reaction rates are calculated with a brute-force method in which the coefficients are calculated as

$$S_i = \frac{(\Delta\tau/\tau)}{(\Delta k_i/k_i)} \quad (2)$$

where τ is the ignition delay time and k_i is the rate constant of ith reaction. The results of the analysis are shown in Fig. 12. Among the reactions, the H-abstraction by HO_2 from ethanol (R4) is sensitive for temperatures of both 800 and 1100 K.

$$CH_3CH_2OH + HO_2 = CH_3CHOH + H_2O_2 \quad (R4a)$$

$$= CH_2CH_2OH + H_2O_2 \quad (R4b)$$

The importance of $CH_3CH_2OH + HO_2$ (R4) for ethanol ignition at medium temperature has been noted earlier [12–14,17,60]. As discussed above, the rate of this reaction is estimated by analogy to

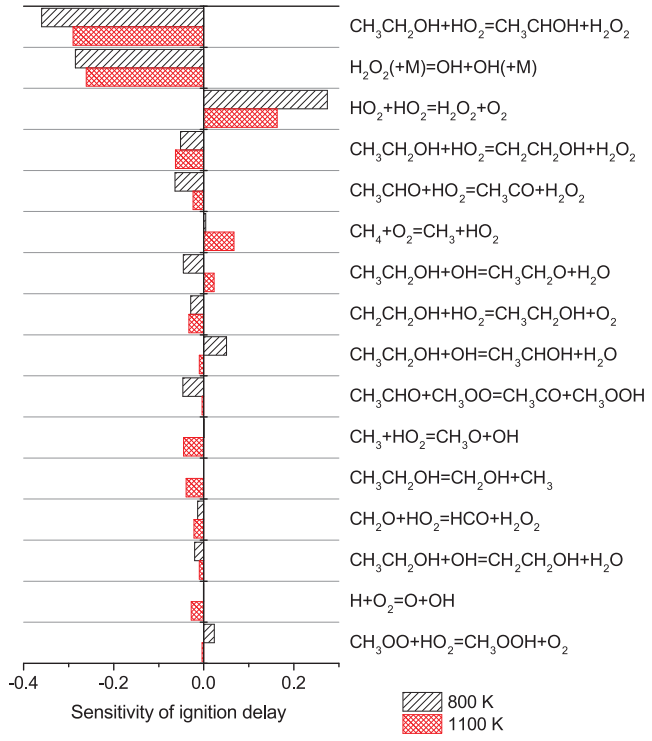

Fig. 12. Sensitivity of ignition delay time prediction to reaction rate constant. The coefficients were calculated as $S_i = (\Delta\tau/\tau)/(\Delta k_i/k_i)$ for a stoichiometric ethanol/air mixtures at 50 bar.

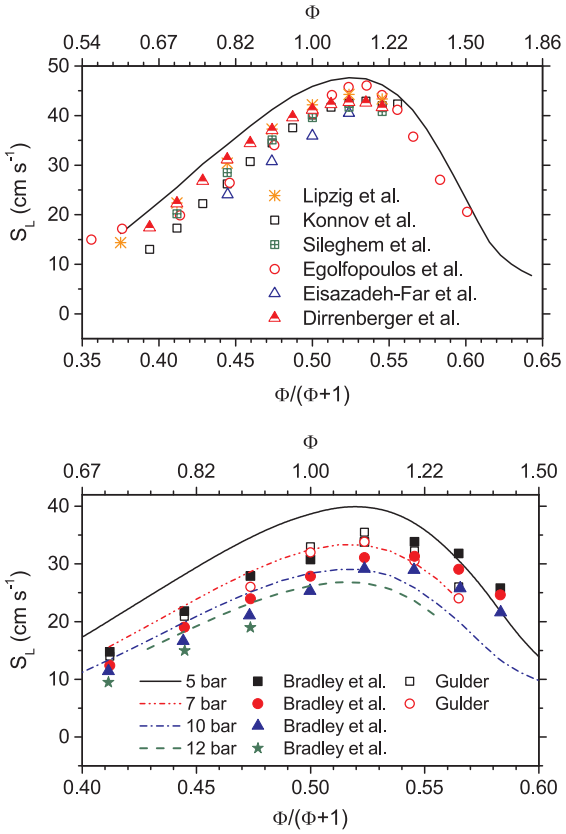

Fig. 13. Laminar burning velocity of ethanol/air mixture. Top: atmospheric pressure and initial temperature of 300 K, Bottom: 5–12 bar pressure and initial temperature of 358 K (350 K for data from Gulder [61]). Experimental results are from Gulder [61], Konnov et al. [64], Bradley et al. [63], van Lipzig et al. [65], Egolfopoulos et al. [62], Eisazadeh-Far et al. [66], Sileghem et al. [67], and Dirrenberger et al. [68].

methanol reactions by Marinov [21] and has a significant uncertainty. To improve model predictions at temperatures below 1000 K, the rate constant of this reaction was modified in [12,13,17], e.g. the overall rate of $CH_3CH_2OH + HO_2$ increased considerably in [17] to improve the predictions for shock-tube conditions. Here, we refrain from optimizing the rate constant of $CH_3CH_2OH + HO_2$, but a reliable determination of the rate constant of this reaction is important to improve our understanding of the ethanol oxidation chemistry at intermediate temperature.

Another source of uncertainty in the present model is the reaction $CH_3CHO + CH_3OO$ (R25), which is important at low temperature (800 K). The rate of this reaction is estimated by analogy with R18 ($CH_3CHO + HO_2$); hence a more accurate determination of this reaction might enhance the accuracy of the model.

4.2.2. Laminar burning velocity

Fig. 13 compares the laminar burning velocity of ethanol/air mixtures calculated by the model with measured data [61–68]. At atmospheric pressure, the model slightly overpredicts the burning velocity but its prediction improves for fuel-rich mixtures. The trend of changes as well as the fuel-air equivalence ratio corresponding to the maximum flame speed are predicted well.

The model is further tested against data obtained at higher pressures of 5–12 bar by Gulder [61] and Bradley et al. [63]. To avoid ethanol condensation at high pressures, the initial temperature had to be increased. While the maximum flame speed at 5 and 7 bar occurred at $\Phi = 1.1$ according to Gulder [61], it was reported at $\Phi = 1.2$ by Bradley et al. [63]. This difference shifts the profiles and causes noticeable scattering between the data in the fuel-rich side. The model overestimates the flame speed at high pressures but its trend is similar to data from Gulder [61].

The sensitivity of the gas flow-rate (in mass unit) to the reaction rate constants is analyzed with Chemkin [54] and the results are shown in Fig. 14. Since the initial temperature and pressure are fixed, the sensitivity coefficients necessarily correlates to the sensitivity of flame speed. Remarkably, no reactions in the ethanol subset of the reaction mechanism exhibits significant sensitivity coefficients. The reactions that are most sensitive in determining the burning velocity are the chain-branching reaction $H + O_2 = O + OH$ R26 and the very exothermic reaction $CO + OH = CO_2 + H$ R27. The decomposition of HCO promotes the burning rate noticeably, whereas its reactions with any of H, OH, or O_2 slow down the burning rate. The C_2 subset is relatively less important in determining the burning velocity. Its most important reactions are

$$C_2H_3 + H(+M) = C_2H_4(+M) \quad \text{(R28)}$$

$$C_2H_2 + H(+M) = C_2H_3(+M) \quad \text{(R29)}$$

The competition between R30 and R31 in consumption of the methyl radicals control the burning velocity of fuel-rich mixtures to a large extent.

$$CH_3 + H(+M) = CH_4(+M) \quad \text{(R30)}$$

$$CH_3 + HO_2 = CH_3\ O + OH \quad \text{(R31)}$$

As can be seen in Fig. 14, almost the same reactions control the flame speed at atmospheric pressure and at higher pressure of 10 bar.

The difference between flame speed measurements and predictions have been reported earlier for ethanol/air mixtures [64,69,70]. Konnov et al. [64] showed that both the models by Konnov et al. [71] and by Saxena and Williams [23] significantly overpredict ethanol laminar burning velocities in lean and near-stoichiometric mixtures. The model by Leplat et al. [25] generally underestimated burning velocities under fuel-rich conditions. Beeckmann et al. [70] tested four chemical kinetic models (Marinov [21], Saxena and Williams [23], Rohl and Peters [72], Leplat et al. [25]) to reproduce ethanol flame speed and found that the

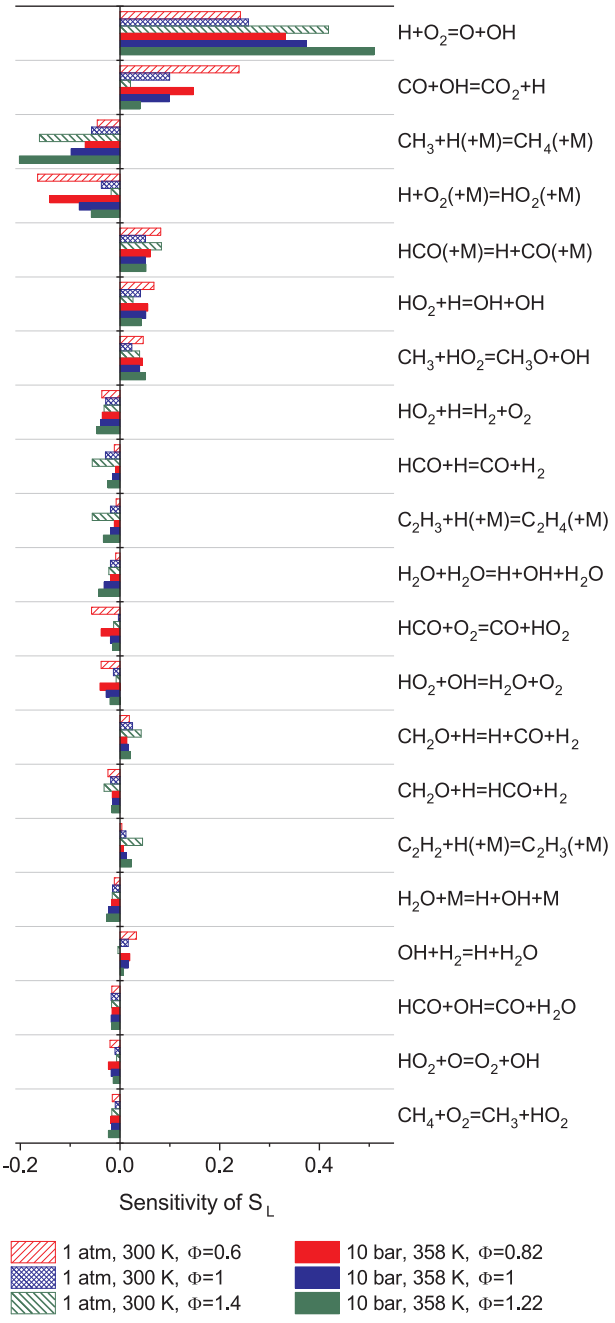

Fig. 14. Sensitivity of flame speed of ethanol/air mixture at 1 atm and 10 bar pressures and the initial temperatures of 300 and 358 K, respectively.

model of Leplat et al. [25] compared better with the measurements at atmospheric pressure, but all the models underpredicted the data at high pressure. In another study by Christensen et al. [69], the over-prediction problem for both ethanol and acetaldehyde flame speed was reported for the models of [23,71]. Christensen et al. [69] analysed the sensitivity of the mechanism by Leplat et al. [25] and found R28 and R29 to be controlling for both ethanol and acetaldehyde flames, similar to the finding here for ethanol flames.

5. Conclusion

Ethanol pyrolysis and oxidation were investigated in a laminar flow reactor at 50 bar pressure and temperatures of 600–900 K. The onset temperature of ethanol oxidation was found to be 700–725 K for a wide range of stoichiometries (Φ = 0.1–43). In pyrolysis experiments, the decomposition of ethanol was detected above 850 K. A detailed chemical kinetic model was developed for ethanol oxidation and pyrolysis. The modelling results agreed well with the measured onset temperature of reaction as well as the concentration of most components after ignition. The model was also used to predict the ignition delay time and flame speed of ethanol. Modelling results agreed well with the literature ignition delays above 900 K. Below 900 K, the model overpredicted ignition delays from shock tubes, possibly due to device-dependent non-idealities encountered in operating shock tubes for long residence times. The flame speeds were slightly overpredicted by the model, most pronounced for fuel-lean mixtures. The present flow reactor data can be used to validate kinetic models at intermediate temperature and elevated pressures. More accurate determination of the key reactions identified here will be helpful in extending the model validity for further applications.

Acknowledgement

Funding from the European Graduate School as well as MAN Diesel & Turbo is gratefully acknowledged. This work was supported by HERCULES–2 under the European Union's Horizon 2020 research and innovation programme.

Appendix A. Supplementary data

Tabulated data from flow-reactor experiments are provided. The detailed mechanism is also attached. Supplementary data associated with this article can be found, in the online version, at http://dx.doi.org/10.1016/j.fuel.2017.12.085.

References

[1] Kohse-Höinghaus K, Oßwald P, Cool TA, Kasper T, Hansen N, Qi F, et al. Biofuel combustion chemistry: from ethanol to biodiesel. Angew Chem, Int Ed 2010;49:3572–97.
[2] Chen H, Shi-Jin S, Jian-Xin W. Study on combustion characteristics and PM emission of diesel engines using ester–ethanol–diesel blended fuels. Proc Combust Inst 2007;31:2981–9.
[3] Sakai S, Rothamer D. Effect of ethanol blending on particulate formation from premixed combustion in spark-ignition engines. Fuel 2017;196:154–68.
[4] Agarwal AK. Biofuels (alcohols and biodiesel) applications as fuels for internal combustion engines. Prog Energy Combust Sci 2007;33:233–71.
[5] Bo Z, Weibiao F, Jingsong G. Study of fuel consumption when introducing DME or ethanol into diesel engine. Fuel 2006;85:778–82.
[6] de Menezes EW, da Silva R, Cataluna R, Ortega RJ. Effect of ethers and ether/ethanol additives on the physicochemical properties of diesel fuel and on engine tests. Fuel 2006;85:815–22.
[7] Yao C, Yang X, Roy Raine R, Cheng C, Tian Z, Li Y. The effects of MTBE/ethanol additives on toxic species concentration in gasoline flame. Energy Fuels 2009;23:3543–8.
[8] Yao M, Zheng Z, Liu H. Progress and recent trends in homogeneous charge compression ignition (HCCI) engines. Prog Energy Combust Sci 2009;35:398–437.
[9] Li J, Kazakov A, Dryer FL. Ethanol pyrolysis experiments in a variable pressure flow reactor. Int J Chem Kinet 2001;33:859–67.
[10] Haas FM, Chaos M, Dryer FL. Low and intermediate temperature oxidation of ethanol and ethanol – PRF blends: an experimental and modeling study. Combust Flame 2009;156:2346–50.
[11] Lee D, Hochgreb S, Keck JC. Autoignition of alcohols and ethers in a rapid compression machine. SAE Tech. Pap. 932755; 1993.
[12] Mittal G, Burke SM, Davies VA, Parajuli B, Metcalfe WK, Curran HJ. Autoignition of ethanol in a rapid compression machine. Combust Flame 2014;161:1164–71.
[13] Lee C, Vranckx S, Heufer KA, Khomik SV, Uygun Y, Olivier H, et al. On the chemical kinetics of ethanol oxidation: shock tube, rapid compression machine and detailed modeling study. Z Phys Chem 2012;226:1–28.
[14] Barraza-Botet CL, Wagnon SW, Wooldridge MS. Combustion chemistry of ethanol: ignition and speciation studies in a rapid compression facility. J Phys Chem A 2016;120:7408–18.
[15] Noorani KE, Akih-Kumgeh B, Bergthorson JM. Comparative high temperature shock tube ignition of C1–C4 primary alcohols. Energy Fuels 2010;24:5834–43.
[16] Heufer KA, Olivier H. Determination of ignition delay times of different hydrocarbons in a new high pressure shock tube. Shock Waves 2010;20:307–16.
[17] Cancino LR, Fikri M, Oliveira AAM, Schulz C. Measurement and chemical kinetics modeling of shock-induced ignition of ethanol-air mixtures. Energy Fuels 2010;24:2830–40.
[18] Dunphy MP, Patterson PM, Simmie JM. High-temperature oxidation of ethanol. Part 2. –kinetic modelling. J Chem Soc, Faraday Trans 1991;87:2549–59.

[19] Norton TS, Dryer FL. The flow reactor oxidation of C1-C4 alcohols and MTBE. Symp Combust 1991;23:179–85.
[20] Norton TS, Dryer FL. An experimental and modeling study of ethanol oxidation-kinetics in an atmospheric-pressure flow reactor. Int J Chem Kinet 1992;24:319–44.
[21] Marinov NM. A detailed chemical kinetic model for high temperature ethanol oxidation. Int J Chem Kinet 1999;31:183–220.
[22] Li J, Kazakov A, Dryer FL. Experimental and numerical studies of ethanol decomposition reactions. J Phys Chem A 2004;108:7671–80.
[23] Saxena P, Williams FA. Numerical and experimental studies of ethanol flames. Proc Combust Inst 2007;31:1149–56.
[24] Frassoldati A, Cuoci A, Faravelli T, Ranzi E. Kinetic modeling of the oxidation of ethanol and gasoline surrogate mixtures. Combust Sci Technol 2010;182:653–67.
[25] Leplat N, Dagaut P, Togbé C, Vandooren J. Numerical and experimental study of ethanol combustion and oxidation in laminar premixed flames and in jet-stirred reactor. Combust Flame 2011;158:705–25.
[26] Rasmussen CL, Hansen J, Marshall P, Glarborg P. Experimental measurements and kinetic modeling of $CO/H_2/O_2/NO$, conversion at high pressure. Int J Chem Kinet 2008;40:454–80.
[27] Rasmussen CL, Jakobsen JG, Glarborg P. Experimental measurements and kinetic modeling of CH_4/O_2 and $CH_4/C_2H_6/O_2$ conversion at high pressure. Int J Chem Kinet 2008;40:778–807.
[28] Rasmussen CL, Wassard KH, Dam-Johansen K, Glarborg P. Methanol oxidation in a flow reactor: implications for the branching ratio of the $CH_3OH + OH$ reaction. Int J Chem Kinet 2008;40:423–41.
[29] Gimenez-Lopez J, Rasmussen CL, Alzueta MU, Gao Y, Marshall P, Glarborg P. Experimental and kinetic modeling study of C_2H_4 oxidation at high pressure. Proc Combust Inst 2009;32:367–75.
[30] Aranda V, Christensen JM, Alzueta MU, Glarborg P, Gersen S, Gao Y, et al. Experimental and kinetic modeling study of methanol ignition and oxidation at high pressure. Int J Chem Kinet 2013;45:283–94.
[31] Hashemi H, Christensen JM, Gersen S, Glarborg P. Hydrogen oxidation at high pressure and intermediate temperatures: experiments and kinetic modeling. Proc Combust Inst 2015;35:553–60.
[32] Hashemi H, Christensen JM, Gersen S, Levinsky H, Klippenstein SJ, Glarborg P. High-pressure oxidation of methane. Combust Flame 2016;172:349–64.
[33] Hashemi H, Jacobsen JG, Rasmussen CT, Christensen JM, Glarborg P, Gersen S, et al. High-pressure oxidation of ethane. Combust Flame 2017;182:150–66.
[34] Christensen JM, Jensen PA, Jensen AD. Effects of feed composition and feed impurities in the catalytic conversion of syngas to higher alcohols over alkali-promoted cobalt-molybdenum sulfide. Ind Eng Chem Res 2011;50:7949–63.
[35] Gimenez-Lopez J, Rasmussen C, Hashemi H, Alzueta M, Gao Y, Marshall P, et al. Experimental and kinetic modeling study of C_2H_2 oxidation at high pressure. Int J Chem Kinet 2016;48:724–38.
[36] Song Y, Hashemi H, Christensen JM, Zou C, Marshall P, Glarborg P. Ammonia oxidation at high pressure and intermediate temperatures. Fuel 2016;181:358–65.
[37] Hashemi H, Glarborg P, Marshall P. Development and validation of a kinetic model for acetaldehyde oxidation over a wide pressure and temperature range, in preparation; 2018.
[38] Sivaramakrishnan R, Su M-C, Michael JV, Klippenstein SJ, Harding LB, Ruscic B. Rate constants for the thermal decomposition of ethanol and its bimolecular reactions with OH and D: reflected shock tube and theoretical studies. J Phys Chem A 2010;114:9425–39.
[39] Zheng J, Truhlar DG. Multi-path variational transition state theory for chemical reaction rates of complex polyatomic species: ethanol + OH reactions. Faraday Discuss 2012;157:59–88.
[40] Xu ZF, Park J, Lin MC. Thermal decomposition of ethanol. III. A computational study of the kinetics and mechanism for the $CH_3 + C_2H_5OH$ reaction. J Chem Phys 2004;120:6593–9.
[41] Dames EE. Master equation modeling of the unimolecular decompositions of alpha-hydroxyethyl (CH_3CHOH) and ethoxy (CH_3CH_2O) radicals. Int J Chem Kinet 2014;46:176–88.
[42] Labbe NJ, Sivaramakrishnan R, Klippenstein SJ. The role of radical + fuel-radical well-skipping reactions in ethanol and methylformate low-pressure flames. Proc Combust Inst 2015;35:447–55.
[43] Sivaramakrishnan R. Personal Communication; 2014.
[44] da Silva G, Bozzelli JW, Liang L, Farrell JT. Ethanol oxidation: kinetics of the alpha-hydroxyethyl radical + O_2 reaction. J Phys Chem A 2009;113:8923–33.
[45] Senosiain JP, Klippenstein SJ, Miller JA. Reaction of ethylene with hydroxyl radicals: a theoretical study. J Phys Chem A 2006;110:6960–70.
[46] Xu ZF, Xu K, Lin MC. Ab initio kinetics for decomposition/isomerization reactions of C_2H_5O radicals. ChemPhysChem 2009;10:972–82.
[47] Zador J, Fernandes RX, Georgievskii Y, Meloni G, Taatjes CA, Miller JA. The reaction of hydroxyethyl radicals with O_2: a theoretical analysis and experimental product study. Proc Combust Inst 2009;32:271–7.
[48] Xu ZF, Xu K, Lin MC. Thermal decomposition of ethanol. 4. Ab initio chemical kinetics for reactions of H atoms with CH_3CH_2O and CH_3CHOH radicals. J Phys Chem A 2011;115:3509–22.
[49] Wu C-W, Matsui H, Wang N-S, Lin MC. Shock tube study on the thermal decomposition of ethanol. J Phys Chem A 2011;115:8086–92.
[50] Kiecherer J, Bänsch C, Bentz T, Olzmann M. Pyrolysis of ethanol: a shock-tube/TOF-MS and modeling study. Proc Combust Inst 2015;35:465–72.
[51] Carr SA, Blitz MA, Seakins PW. Site-specific rate coefficients for reaction of OH with ethanol from 298 to 900 K. J Phys Chem A 2011;115:3335–45.
[52] Xu S, Lin M. Theoretical study on the kinetics for OH reactions with CH_3OH and C_2H_5OH. Proc Combust Inst 2007;31:159–66.
[53] Stranic I, Pang GA, Hanson RK, Golden DM, Bowman CT. Shock tube measurements of the rate constant for the reaction ethanol plus OH. J Phys Chem A 2014;118:822–8.
[54] Ansys 17.2 Chemkin-Pro; 2017.
[55] Yamada T, Bozzelli JW, Lay T. Kinetic and thermodynamic analysis on OH addition to ethylene: adduct formation, isomerization, and isomer dissociations. J Phys Chem A 1999;103:7646–55.
[56] Srinivasan NK, Su M-C, Michael JV. Reflected shock tube studies of high-temperature rate constants for $OH + C_2H_2$ and $OH + C_2H_4$. Phys Chem Chem Phys 2007;9:4155–63.
[57] Caralp F, Devolder P, Fittschen C, Gomez N, Hippler H, Mereau R, et al. The thermal unimolecular decomposition rate constants of ethoxy radicals. Phys Chem Chem Phys 1999;1:2935–44.
[58] Dryer FL, Chaos M. Ignition of syngas/air and hydrogen/air mixtures at low temperatures and high pressures: experimental data interpretation and kinetic modeling implications. Combust Flame 2008;152:293–9.
[59] Chaos M, Dryer FL. Chemical-kinetic modeling of ignition delay: considerations in interpreting shock tube data. Int J Chem Kinet 2010;42:143–50.
[60] Herrmann F, Jochim B, Owald P, Cai L, Pitsch H, Kohse-Höinghaus K. Experimental and numerical low-temperature oxidation study of ethanol and dimethyl ether. Combust Flame 2014;161:384–97.
[61] Gulder OL. Laminar burning velocities of methanol, ethanol and isooctane-air mixtures. Symp (Int) Combust, [Proc] 1982;19:275–81.
[62] Egolfopoulos FN, Du DX, Law CK. A study on ethanol oxidation kinetics in laminar premixed flames, flow reactors, and shock tubes. Symp (Int) Combust, [Proc] 1992;24:833–41.
[63] Bradley D, Lawes M, Mansour MS. Explosion bomb measurements of ethanol-air laminar gaseous flame characteristics at pressures up to 1.4 MPa. Combust Flame 2009;156:1462–70.
[64] Konnov A, Meuwissen R, De Goey L. The temperature dependence of the laminar burning velocity of ethanol flames. Proc Combust Inst 2011;33:1011–9.
[65] van Lipzig JPJ, Nilsson EJK, de Goey LPH, Konnov AA. Laminar burning velocities of n-heptane, iso-octane, ethanol and their binary and tertiary mixtures. Fuel 2011;90:2773–81.
[66] Eisazadeh-Far K, Moghaddas A, Al-Mulki J, Metghalchi H. Laminar burning speeds of ethanol/air/diluent mixtures. Proc Combust Inst 2011;33:1021–7.
[67] Sileghem L, Alekseev V, Vancoillie J, Nilsson E, Verhelst S, Konnov A. Laminar burning velocities of primary reference fuels and simple alcohols. Fuel 2014;115:32–40.
[68] Dirrenberger P, Glaude P-A, Bounaceur R, Le Gall H, da Cruz AP, Konnov A, et al. Laminar burning velocity of gasolines with addition of ethanol. Fuel 2014;115:162–9.
[69] Christensen M, Abebe MT, Nilsson EJK, Konnov AA. Kinetics of premixed acetaldehyde + air flames. Proc Combust Inst 2015;35:499–506.
[70] Beeckmann J, Cai L, Pitsch H. Experimental investigation of the laminar burning velocities of methanol, ethanol, n-propanol, and n-butanol at high pressure. Fuel 2014;117:340–50.
[71] Konnov A. Implementation of the NCN pathway of prompt-NO formation in the detailed reaction mechanism. Combust Flame 2009;156:2093–105.
[72] Rohl O, Peters N. A reduced mechanism for ethanol oxidation. In: Eur Combust Meet, Vienna; 2009.